MECSOL Joinville 2017

April 26-28, 2017
Joinville, Santa Catarina, Brazil

A Variational Constitutive Model for the Viscoelastic Behavior of Biological Materials under AFM Indentation Tests

Thiago A. Carniel
GRANTE, Department of Mechanical Engineering.
Federal University of Santa Catarina, Florianópolis, SC, Brazil.
carnielta@gmail.com

Eduardo A. Fancello
GRANTE, Department of Mechanical Engineering.
LEBm, University Hospital.
Federal University of Santa Catarina, Florianópolis, SC, Brazil.
eduardo.fancello@ufsc.br

ABSTRACT

The present manuscript proposes a finite strain phenomenological model applied to the modeling of the viscoelastic behavior of biological materials in conjunction with finite element simulations of atomic force microscopy (AFM) indentations. The proposed model is formulated within a thermodynamically consistent framework based on a variational constitutive approach. In order to assess the applicability of the model, a numerical investigation of the local viscoelastic behavior of living cells is performed and compared with experimental data. The numerical procedure developed in this study seems to provide an appropriate numerical environment for a better understanding of the viscoelastic behavior of biological materials under nanoindentation experiments.

Keywords: Living cells, Finite viscoelasticity, Variational constitutive modeling, AFM nanoindentation.

1 INTRODUCTION

In many connective tissues, such as tendons, ligaments and cartilage, the mechanical responses to external loadings are highly dependent on their hierarchical microstructures, cellular organization and interactions between one another [1]. In this context, the biological microstructures play a remarkable role in the biomechanical behavior.

Through the tissues hierarchies, each microstructural phase may be subjected to complex mechanical environment, experiencing finite strains and presenting particular nonlinear behaviors, including viscoelastic effects. Therefore, the knowledge and correct interpretation of the mechanical responses of the microstructural phases certainly constitutes useful information for a better understanding of the multiscale mechanics of the tissue.

Several measurement techniques have been employed to assess the micromechanical responses of biological materials, where the atomic force microscopy (AFM) indentation is the most comprehensive of them. Also known as nanoindentation tests, the AFM indentation experiments are employed to assess the micromechanical responses of a large range of biological materials, e.g.: living cells [2–5], collagen fibers [6], collagen fibrils [7], bones [8], skin [9] and others. In a numerical perspective, the AFM indentations provide a convenient structure to finite element simulations. For

instance, whereas the biological sample is modeled locally as a homogenous medium, the tip of the indenter can be considered a rigid body.

With these motivations in mind, the present work proposes a finite strain viscoelastic model in order to represent the micromechanical responses of biological materials in conjunction with finite element simulations of nanoindentation tests. The proposed model is formulated in a thermodynamically consistent framework based on the variational formalism addressed in [10–13].

The manuscript is organized as follows. In Section 2 is presented the theoretical background related to the variational constitutive modeling of a viscoelastic material subjected to finite strains. Aiming at finite element simulations, this section also addresses the discretized version of the continuum constitutive equations, leading to the local algorithm of the material model. As a case of study, a numerical investigation of the local stiffness and energetic dissipation of fibroblast cells is performed. Accordingly, a set of numerical results related to these analyses are shown in Section 3. Finally, some particularities of the model and further discussions regarding to the viscoelastic behavior of cells are highlighted in Section 4.

2 CONSTITUTIVE MODELING APPROACH

2.1 Kinematics and Thermodynamic Potentials

The classic multiplicative decomposition of the deformation gradient is proposed herein to separate de elastic and viscous contributions:

$$\mathbf{F} = \mathbf{F}^{\mathrm{e}}\mathbf{F}^{\mathrm{v}}, \quad J^{\mathrm{e}} := \det\left(\mathbf{F}^{\mathrm{e}}\right) > 0, \quad J^{\mathrm{v}} := \det\left(\mathbf{F}^{\mathrm{v}}\right) > 0\,. \tag{2.1}$$

In view of decomposition (2.1), the total, elastic and viscous right Cauchy-Green strain tensors are introduced as,

$$\mathbf{C} := \mathbf{F}^{\mathrm{T}}\mathbf{F}, \quad \mathbf{C}^{\mathrm{e}} := \mathbf{F}^{\mathrm{e}^{\mathrm{T}}}\mathbf{F}^{\mathrm{e}}, \quad \mathbf{C}^{\mathrm{v}} := \mathbf{F}^{\mathrm{v}^{\mathrm{T}}}\mathbf{F}^{\mathrm{v}}\,. \tag{2.2}$$

The symmetric part of the velocity gradient $\mathbf{l} := \dot{\mathbf{F}}\mathbf{F}^{-1}$ defines the spatial rate of deformation $\mathbf{d} := \mathrm{sym}\left(\mathbf{l}\right)$. However, in the present modeling approach, the viscous rate of deformation is defined by,

$$\mathbf{d}^{\mathrm{v}} := \mathrm{sym}\left(\mathbf{l}^{\mathrm{v}}\right) = \mathbf{l}^{\mathrm{v}} = \dot{\mathbf{F}}^{\mathrm{v}}\mathbf{F}^{\mathrm{v}^{-1}}, \qquad \mathrm{skew}\left(\mathbf{l}^{\mathrm{v}}\right) = \mathbf{0}, \tag{2.3}$$

where the assumption of null viscous spin is used [14].

The constitutive modeling of dissipative materials can be cast in a thermodynamically consistent framework by defining the Helmholtz free energy ψ, and a so-called dissipation pseudo-potential ϕ [15,16].

The proposed viscoelastic model is formulated in view of the well-known standard solid rheological assembly, where further details can be found in [17]. According to this and choosing $\mathbf{F}^{\mathrm{v}}$

as an internal variable, the Helmholtz free energy and the dissipation potential are formally introduced as

$$\psi \coloneqq \psi^{\infty}\left(\mathbf{C}\right) + \psi^{\mathrm{e}}\left(\mathbf{C}^{\mathrm{e}}\right), \quad \phi \coloneqq \phi^{\mathrm{v}}\left(\mathbf{d}^{\mathrm{v}}\right), \tag{2.4}$$

where the superscript ∞ represents the time-independent response. Moreover, the arguments of potentials (2.4) are objective tensors [18].

2.2 Variational Constitutive Approach

The variational constitutive modeling approach proposed herein is guided by the variational formalism addressed in [10–13]. In view of the thermodynamic potentials (2.4), one can define a rate potential in the form [10,11]:

$$\mathcal{P}\left(\dot{\mathbf{F}}, \dot{\mathbf{F}}^{\mathrm{v}}\right) \coloneqq \dot{\psi}\left(\dot{\mathbf{F}}, \dot{\mathbf{F}}^{\mathrm{v}}\right) + \phi^{\mathrm{v}}\left(\mathbf{d}^{\mathrm{v}}\right). \tag{2.5}$$

The incremental counterpart of potential (2.5) relies on a proper numerical integration scheme. Considering an increment of time $\Delta t = t_{n+1} - t_n$, a possible general expression for the incremental potential is given by

$$\mathcal{P}_{\mathrm{inc}}\left(\mathbf{F}_{n+1}, \mathbf{F}^{\mathrm{v}}_{n+1}\right) \coloneqq \psi\left(\mathbf{F}_{n+1}, \mathbf{F}^{\mathrm{v}}_{n+1}\right) - \psi\left(\mathbf{F}_{n}, \mathbf{F}^{\mathrm{v}}_{n}\right) + \Delta t\left[\phi^{\mathrm{v}}\left(\breve{\mathbf{d}}^{\mathrm{v}}\right)\right]\Big|_{t_{n+\vartheta}}, \tag{2.6}$$

where the variables $\breve{\mathbf{d}}^{\mathrm{v}}\left(\breve{\mathbf{F}}^{\mathrm{v}}\right)$ and $\breve{\mathbf{F}}^{\mathrm{v}}$ are discrete approximations for the rates $\mathbf{d}^{\mathrm{v}}$ and $\dot{\mathbf{F}}^{\mathrm{v}}$, respectively. One can note that the dissipation potential ϕ^{v} is evaluated at an intermediate time $t_{n+\vartheta}$ inside of the time increment, where the parameter $\vartheta \in \left[0,1\right]$ is closely related to the discretization rule employed in $\breve{\mathbf{F}}^{\mathrm{v}}$. Therefore, the consistency of the incremental form (2.6) can be verified if $\Delta t \to 0 \Rightarrow \mathcal{P}_{\mathrm{inc}} = \mathcal{P}$. In view of the incremental potential, the variational updates algorithm is composed by two main procedures:

1. The incremental rate of the internal variable is solution of the variational principle

$$\breve{\mathbf{F}}^{\mathrm{v}\,\mathrm{opt}} = \arg \inf_{\breve{\mathbf{F}}^{\mathrm{v}}} \mathcal{P}_{\mathrm{inc}}\big|_{\mathbf{F}_{n+1}=\mathrm{cte}}. \tag{2.7}$$

2. Once the optimal solution is obtained in (2.7), the incremental stress is updated by

$$\mathbf{P}_{n+1} = \left.\frac{\partial \mathcal{P}_{\mathrm{inc}}}{\partial \mathbf{F}_{n+1}}\right|_{\breve{\mathbf{F}}^{\mathrm{v}} = \breve{\mathbf{F}}^{\mathrm{v}\,\mathrm{opt}}}. \tag{2.8}$$

The variational principle (2.7) defines a new potential, namely the reduced incremental potential $\mathcal{P}_{\text{inc}}^{\text{red}}$, which is only function of $\mathbf{F}_{n+1}$. The total derivative of $\mathcal{P}_{\text{inc}}^{\text{red}}$ with respect to $\mathbf{F}_{n+1}$ also results in the first Piola-Kirchhoff stress tensor,

$$\mathbf{P}_{n+1} = \frac{\mathrm{d}\mathcal{P}_{\text{inc}}^{\text{red}}}{\mathrm{d}\mathbf{F}_{n+1}}, \quad \text{where} \quad \mathcal{P}_{\text{inc}}^{\text{red}}\left(\mathbf{F}_{n+1}\right) \coloneqq \inf_{\breve{\mathbf{F}}^{\text{v}}} \mathcal{P}_{\text{inc}}\left(\mathbf{F}_{n+1}, \mathbf{F}_{n+1}^{\text{v}}\right). \tag{2.9}$$

The reduced incremental potential grants remarkable numerical features. For example, the constitutive problem presents a hyperelastic behavior inside of the time increment, the consistent material tangent modulus keeps major symmetry and also exist the possibility of investigate the uniqueness of solution [10,12,13,19]. Accordingly, this variational approach becomes a mathematically elegant and numerically robust tool to formulate and solve the constitutive equations.

2.2.1 Internal Variable Updates Algorithm

In the present work, the continuum rates (2.3) are incrementally approximated by the classical Euler scheme:

$$\mathbf{d}^{\text{v}} \approx \breve{\mathbf{d}}^{\text{v}} = \breve{\mathbf{F}}^{\text{v}} \mathbf{F}_{n+\vartheta}^{\text{v}^{-1}}, \quad \dot{\mathbf{F}}^{\text{v}} \approx \breve{\mathbf{F}}^{\text{v}} = \frac{1}{\Delta t}\left(\mathbf{F}_{n+1}^{\text{v}} - \mathbf{F}_{n}^{\text{v}}\right), \tag{2.10}$$

in which $\mathbf{F}_{n+\vartheta}^{\text{v}} = \left(1-\vartheta\right)\mathbf{F}_{n}^{\text{v}} + \vartheta\mathbf{F}_{n+1}^{\text{v}}$ defines a linear interpolation of the internal variable within the time increment [20]. Assuming $\vartheta = 1$, that represents a fully implicit rule, one can define from equations (2.10) the following updating rule:

$$\mathbf{F}_{n+1}^{\text{v}} = \left(\mathbf{I} - \Delta t\, \breve{\mathbf{d}}^{\text{v}}\right)^{-1} \mathbf{F}_{n}^{\text{v}}, \tag{2.11}$$

where $\mathbf{I}$ is the second order identity tensor. Moreover, in the present modeling approach, the viscous flow is considered incompressible. Therefore, the minimum principle (2.7) can be rewritten as

$$\breve{\mathbf{d}}^{\text{v}^{\text{opt}}} = \arg \inf_{\breve{\mathbf{d}}^{\text{v}} \in \mathcal{I}so} \mathcal{P}_{\text{inc}}\Big|_{\mathbf{F}_{n+1}=\text{cte}}, \tag{2.12}$$

where $\mathcal{I}so \coloneqq \left\{\breve{\mathbf{d}}^{\text{v}} \in \mathcal{S}ym \middle| \det\left[\mathbf{F}_{n+1}^{\text{v}}\left(\breve{\mathbf{d}}^{\text{v}}\right)\right] = 1\right\}$ represents the isochoric viscous space and $\mathcal{S}ym$ the space of symmetric second order tensors. The kinematic constraint $J_{n+1}^{\text{v}} \coloneqq \det\left(\mathbf{F}_{n+1}^{\text{v}}\right) = 1$ is taking into account by means of the Lagrangian functional

$$\mathcal{L}\left(\breve{\mathbf{d}}^{\text{v}}, \gamma_{n+1}\right) \coloneqq \mathcal{P}_{\text{inc}} + \gamma_{n+1}\left(J_{n+1}^{\text{v}} - 1\right), \tag{2.13}$$

where γ_{n+1} is a Lagrange multiplier. Consequently, the minimum principle (2.12) can be rewritten as an unconstrained problem, such that:

$$\left(\breve{\mathbf{d}}^{\mathrm{v}}, \gamma_{n+1}\right)^{\mathrm{opt}} = \arg \underset{\left(\breve{\mathbf{d}}^{\mathrm{v}}, \gamma_{n+1}\right)}{\mathrm{stat}} \mathcal{L}\big|_{\mathbf{F}_{n+1}=\mathrm{cte}} . \tag{2.14}$$

The solution of the variational principle (2.14) defines the internal variable updates algorithm. Once the optimum solution for the incremental rate $\breve{\mathbf{d}}^{\mathrm{v}}$ is found, the internal variable is updated by equation (2.11). The solution strategy employed in this work to solve the optimization problem (2.14) is based on the full Newton-Raphson procedure [21].

2.2.2 Stress Evaluation and Consistent Material Tangent Modulus

Once the solution of (2.14) is obtained, the stress can be updated as follows. In view of (2.8), the incremental first Piola-Kirchhoff stress tensor is given by

$$\mathbf{P}_{n+1} = \frac{\partial \mathcal{P}_{\mathrm{inc}}}{\partial \mathbf{F}_{n+1}}\bigg|_{\breve{\mathbf{d}}^{\mathrm{v}}=\breve{\mathbf{d}}^{\mathrm{v}^{\mathrm{opt}}}} = \frac{\partial \psi}{\partial \mathbf{F}_{n+1}}\bigg|_{\breve{\mathbf{d}}^{\mathrm{v}}=\breve{\mathbf{d}}^{\mathrm{v}^{\mathrm{opt}}}} = \left(\frac{\partial \psi^{\infty}}{\partial \mathbf{F}_{n+1}} + \frac{\partial \psi^{\mathrm{e}}}{\partial \mathbf{F}_{n+1}}\right)\bigg|_{\breve{\mathbf{d}}^{\mathrm{v}}=\breve{\mathbf{d}}^{\mathrm{v}^{\mathrm{opt}}}} . \tag{2.15}$$

The partial derivatives of the Helmholtz strain energies in relation to $\mathbf{F}_{n+1}$ result in

$$\mathbf{P}_{n+1} = \mathbf{F}_{n+1}\mathbf{S}_{n+1}, \quad \mathbf{S}_{n+1} := \mathbf{S}^{\infty}_{n+1} + \mathbf{F}^{\mathrm{v}^{-1}}_{n+1}\mathbf{S}^{\mathrm{e}}_{n+1}\mathbf{F}^{\mathrm{v}^{-\mathrm{T}}}_{n+1} , \tag{2.16}$$

where $\mathbf{S}_{n+1}$ is the second Piola-Kirchhoff stress tensor. In addition, the time-independent and the elastic second Piola stresses are defined as,

$$\mathbf{S}^{\infty}_{n+1} := 2\frac{\partial \psi^{\infty}}{\partial \mathbf{C}_{n+1}}, \quad \mathbf{S}^{\mathrm{e}}_{n+1} := 2\frac{\partial \psi^{\mathrm{e}}}{\partial \mathbf{C}^{\mathrm{e}}_{n+1}} . \tag{2.17}$$

Within the framework of a conventional nonlinear finite element code, the consistent tangent modulus must be provided [22]. Taking into account a total Lagrangian formulation [23], the linearization of the equilibrium equations results in the material tangent modulus,

$$\mathbb{C}_{n+1} := 2\frac{\mathrm{d}\mathbf{S}_{n+1}}{\mathrm{d}\mathbf{C}_{n+1}} = 4\frac{\mathrm{d}^2\ \mathcal{P}^{\mathrm{red}}_{\mathrm{inc}}}{\mathrm{d}\mathbf{C}_{n+1}\mathrm{d}\mathbf{C}_{n+1}}, \tag{2.18}$$

where d represents the total derivative operator. It is important to notice that if $\mathcal{P}^{\mathrm{red}}_{\mathrm{inc}}$ is a convex potential of $\mathbf{C}_{n+1}$, the major symmetry of the tensor $\mathbb{C}_{n+1}$ is guaranteed.

2.3 Choice of Viscoelastic Potentials

As a case of study, a numerical investigation of the local stiffness and energetic dissipation of living cells is addressed in the next section. Therefore, to model the viscoelastic behavior of cells, the following potentials are proposed:

$$\begin{cases} \psi^{\infty} := \dfrac{\mu^{\infty}}{2}\Big[\operatorname{tr}\Big(\mathbf{C}\Big) - 3\Big] - \mu^{\infty}\ln\Big(J\Big) + \dfrac{\kappa^{\infty}}{2}\Big[\ln\Big(J\Big)\Big]^2 \\ \psi^{\mathrm{e}} := \dfrac{\mu^{\mathrm{e}}}{2}\Big[\operatorname{tr}\Big(\mathbf{C}^{\mathrm{e}}\Big) - 3\Big] - \mu^{\mathrm{e}}\ln\Big(J^{\mathrm{e}}\Big) \\ \phi^{\mathrm{v}} := \dfrac{\eta^{\mathrm{v}}}{2}\mathbf{d}^{\mathrm{v}} : \mathbf{d}^{\mathrm{v}} \end{cases}, \tag{2.19}$$

where $\left\{\mu^{\infty}, \kappa^{\infty}, \mu^{\mathrm{e}}, \eta^{\mathrm{v}}\right\}$ are the constitutive parameters. In equation (2.19), the strain energies are represented by the Neo-Hookean model [24], and the dissipation potential possesses a simple quadratic form in the viscous rate of deformation.

3 RESULTS

The finite element analysis presented herein aim to simulate cyclic AFM indentation tests. The numerical simulations follow the experimental protocol carried out by [4] in fibroblast cells. In Figure 1 are shown details on the finite element model. The proposed model are composed by a rigid $1.98\ \mu\mathrm{m}$ diameter spherical indenter and a numerical sample with diameter of $10\ \mu\mathrm{m}$ and height of $4\ \mu\mathrm{m}$. The cell sample is modeled as a homogeneous medium, discretized by $15,000$ linear prismatic elements, where a mesh refinement was performed in the indentation region. Moreover, a quarter symmetry of the sample is considered and the frictionless contact was imposed in the interface between the sample and the rigid indenter. The simulations were performed under an indentation rate of $0.8\ \mu\mathrm{m/s}$.

The finite element simulations were run in the software Abaqus, where the proposed viscoelastic model was implemented into the user-subroutine UMAT.

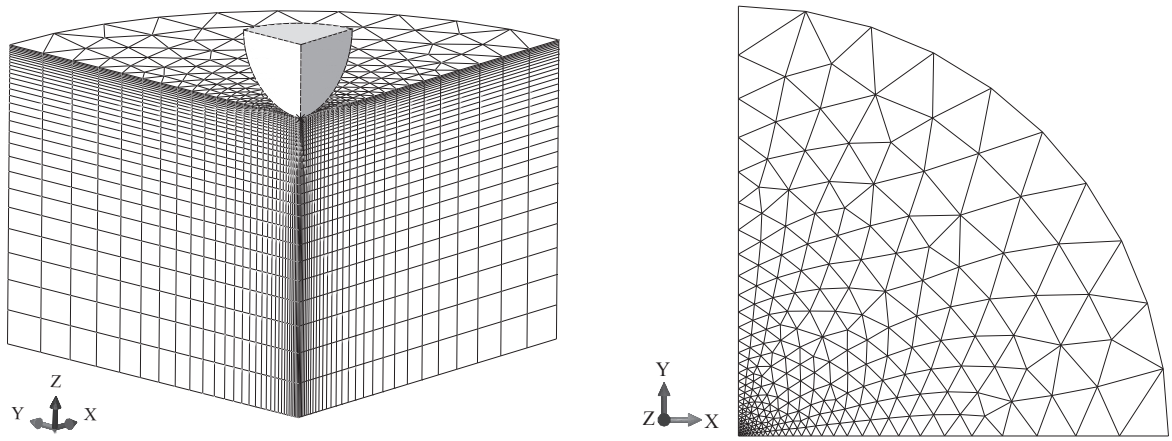

(a) (b)

Figure 1. Finite element model. (a) Perspective view of the model showing the spherical indenter and the cell sample in a quarter symmetry. (b) Top view of the numerical sample, where the mesh refinement is noted in the indentation region.

It is a common practice in the biomechanical analysis of living cells to assess the local stiffness by fitting the AFM indentation experiments to Hertz contact models [25]. In this case, the cell is modeled locally as a linear isotropic (and generally incompressible) material, where the elastic parameter E (Young's modulus) attempts to represent a measure of stiffness. The Hertzian model for a spherical tip is given by,

$$F\left(d\right) = \frac{4E\sqrt{r}}{3\left(1-\nu^2\right)} d^{3/2}, \tag{3.1}$$

where $F\left(d\right)$ is the force-depth relation of the indenter, r is the radius of the tip and E and ν are the linear elastic parameters, represented by the Young's modulus and Poisson's ratio, respectively.

It is important to note that although Hertzian expressions have shown to be excellent shape functions to reproduce nanoindentation curves subjected to finite strains, these expressions are of limited use for modeling the mechanical behavior of cells. The same test performed at different indentation depths generally needs different values $\left\{E,\nu\right\}$ to reproduce the experimental curve. In other words, it is in general not possible to find a unique set $\left\{E,\nu\right\}$ to represent the same material.

Experimental investigations based on Herzian expressions point out the parameter E of fibroblast cells can range from 50 Pa up to 150 kPa onto the cell surface [3,5,26]. Moreover, a log-normal distribution between 10 kPa up to 100 kPa with a mean value of ~ 46 kPa was verified in [5]. In addition, the hysteresis loops under cyclic AFM indentations present large variations depending on the tested point onto the cell surface [27].

Based on this reasoning and the mentioned experimental data found in [3,5,26], the equation (3.1) is employed to retrieve experimental indentation curves with the parameter E equal to 10, 50

and $100\ \mathrm{kPa}$ (see Figure 2(a)). These monotonic curves will provide the experimental basis in order to estimate the constitutive parameters of the proposed viscoelastic model considering three levels of stiffness and energetic dissipations: upper and lower bounds and a mean value.

For each stiffness level, the proposed viscoelastic model was used and its constitutive parameters were estimated in order to reproduce the monotonic experimental curves with three percentages of hystereses: 16%, 33% and 56%. The identification procedure was performed as follows. A fixed ratio $\kappa^{\infty} = 10^2 \mu^{\infty}$ (compressible response) was defined for the time-independent volumetric parameter, and the remaining viscoelastic parameters $\left\{\mu^{\mathrm{e}}, \eta^{\mathrm{v}}\right\}$ were identified in order to reproduce the loading path of the curves for the three percentages of hysteresis.

The force-displacement curves of the indenter resulting from the finite element simulations are displayed in Figure 2(b-d), while the corresponding material parameters are listed in Table 1.

Table 1: Constitutive parameters related to the numerical curves shown in Figure 2.

Model Parameters	ψ^{∞}		ψ^{e}	ϕ^{v}
	μ^{∞} [kPa]	κ^{∞} [kPa]	μ^{e} [kPa]	η^{v} [kPa · s]
Sim. 1	1.1	110	2.4	12.8
Sim. 2	1.1	110	2.6	4.5
Sim. 3	1.1	110	3.8	2.2
Sim. 4	6	600	11	52
Sim. 5	6	600	13	20
Sim. 6	6	600	18	10
Sim. 7	17	1700	17	70
Sim. 8	17	1700	22	28
Sim. 9	17	1700	32	12

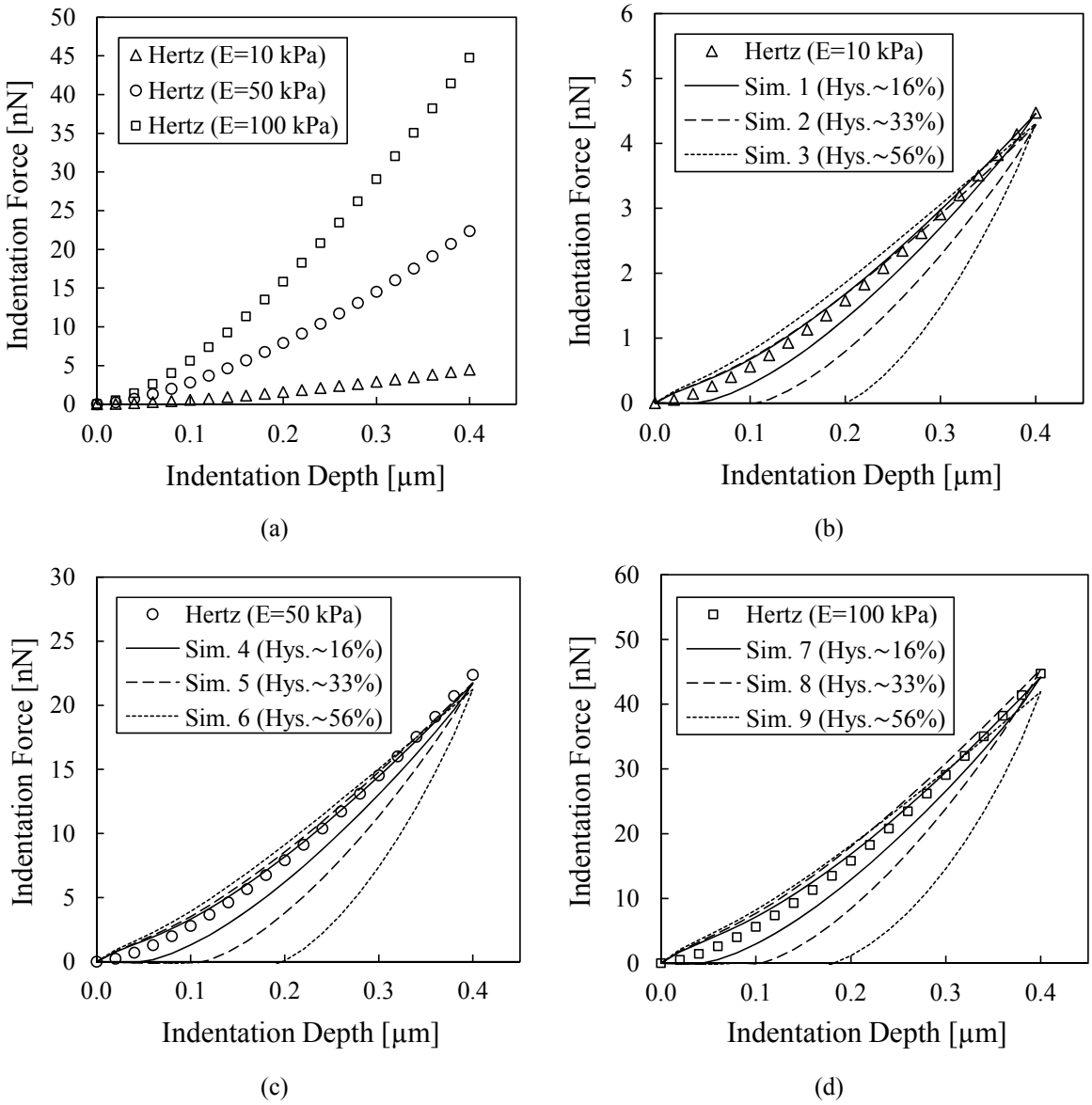

Figure 2. (a) Experimental data reproduced by the Hertz model. (b-d) Finite element predictions for the three levels of energetic dissipation represented by the hysteresis loops.

4 DISCUSSIONS AND FINAL REMARKS

As can be seen from Figure 2, all the numerical simulations were able to reproduce the monotonic loading path of the curves for the three levels of stiffness and for the three percentages of the energetic dissipation proposed. Concerning the hysteresis loops, the characteristic nonlinear shape of the unloading part of the curves show sound agreement with experimental data (compare the numerical results with the experimental curves presented in [4,27]). These numerical results indicate

the model is able to predict the force-displacement curves of the proposed indentation test under different conditions of stiffness and hysteresis onto the cell surface.

In the expression (2.19) for the time-independent strain energy ψ^{∞} the parameter κ^{∞} controls the volume stiffness while μ^{∞} accounts for the distortional one. If incompressibility is to be enforced, κ^{∞} takes values of $\sim \left(10^3 - 10^4\right)\mu^{\infty}$ [24]. However, under physiological conditions, cells can experience large volume changes [28,29]. In the present simulations, a compressible condition was used with $\kappa^{\infty} = 10^2\mu^{\infty}$ (see Table 1). Therefore, even though the proposed model was able to reproduce the experimental curves, further investigations are recommended regarding to the local compressibility behavior of cells.

It is worth noting the mechanical sensitivity of cells to indentation rate and indenter-cell adhesion are issues of research in cell biomechanics [4,27]. In the present case, all simulations were performed under the same indentation rate and considering a frictionless contact condition between sample and indenter. Accordingly, additional numerical and experimental analysis should be carried out in order to investigate these issues.

Finally, the finite element simulation procedure presented in this work seems to provide an appropriate numerical environment for a better understanding of stiffness and energetic dissipation of biological materials. In addition, these procedures may be extended to other biological materials under different indentation conditions.

ACKNOWLEDGMENTS

The authors would like to thank the financial support provided by the Brazilian funding agencies CAPES - (Coordination for the Improvement of Higher Education Personnel) and CNPq - (National Council for Scientific and Technological Development).

REFERENCES

[1] M. Lavagnino, M.E. Wall, D. Little, A.J. Banes, F. Guilak, S.P. Arnoczky, Tendon mechanobiology: Current knowledge and future research opportunities, Journal of Orthopaedic Research. 33 (2015) 813–822.

[2] J. Qi, A.M. Fox, L.G. Alexopoulos, L. Chi, D. Bynum, F. Guilak, A.J. Banes, IL-1beta decreases the elastic modulus of human tenocytes., Journal of Applied Physiology (Bethesda, Md. : 1985). 101 (2006) 189–195.

[3] A. Raman, S. Trigueros, A. Cartagena, a. P.Z. Stevenson, M. Susilo, E. Nauman, S.A. Contera, Mapping nanomechanical properties of live cells using multi-harmonic atomic force microscopy, Nature Nanotechnology. 6 (2011) 809–814.

[4] S. Nawaz, P. Sánchez, K. Bodensiek, S. Li, M. Simons, I.A.T. Schaap, Cell Visco-Elasticity Measured with AFM and Optical Trapping at Sub-Micrometer Deformations, PLoS ONE. 7 (2012).

[5] F.M. Hecht, J. Rheinlaender, N. Schierbaum, W.H. Goldmann, B. Fabry, T.E. Schäffer,

Imaging viscoelastic properties of live cells by AFM: power-law rheology on the nanoscale., Soft Matter. 11 (2015) 4584–4591.

[6] K.E. Aifantis, S. Shrivastava, G.M. Odegard, Transverse mechanical properties of collagen fibers from nanoindentation, Journal of Materials Science: Materials in Medicine. 22 (2011) 1375–1381.

[7] M.P.E. Wenger, L. Bozec, M.A. Horton, P. Mesquida, Mechanical properties of collagen fibrils., Biophysical Journal. 93 (2007) 1255–63.

[8] P.J. Thurner, Atomic force microscopy and indentation force measurement of bone, WIREs Nanomedicine and Nanobiotechnology. 1 (2009) 624–649.

[9] C.A. Grant, P.C. Twigg, D.J. Tobin, Static and dynamic nanomechanical properties of human skin tissue using atomic force microscopy: Effect of scarring in the upper dermis, Acta Biomaterialia. 8 (2012) 4123–4129.

[10] M. Ortiz, L. Stainier, The variational formulation of viscoplastic constitutive updates, Computer Methods in Applied Mechanics and Engineering. 7825 (1999) 419–444.

[11] R. Radovitzky, M. Ortiz, Error estimation and adaptive meshing in strongly nonlinear dynamic problems, Computer Methods in Applied Mechanics and Engineering. 172 (1999) 203–240.

[12] E. Fancello, J.-P. Ponthot, L. Stainier, A variational formulation of constitutive models and updates in non-linear finite viscoelasticity, International Journal for Numerical Methods in Engineering. 65 (2006) 1831–1864.

[13] J.M. Vassoler, L. Reips, E.A. Fancello, A variational framework for fiber-reinforced viscoelastic soft tissues, International Journal for Numerical Methods in Engineering. 89 (2012) 1691–1706.

[14] L. Anand, M.E. Gurtin, A theory of amorphous solids undergoing large deformations , with applications to polymers and metallic glasses, 40 (2003) 1–29.

[15] M. Jirásek, Z. Bazant, Inelastic analysis of structures, John Wiley & Sons, Ltd, 2002.

[16] E.A. de Souza Neto, D. Peric, D.R.J. Owen, Computational Methods for Plasticity: Theory and Applications, 2009.

[17] T.D. Nguyen, R.E. Jones, B.L. Boyce, Modeling the anisotropic finite-deformation viscoelastic behavior of soft fiber-reinforced composites, International Journal of Solids and Structures. 44 (2007) 8366–8389.

[18] M. Gurtin, E. Fried, L. Anand, The mechanics and thermodynamics of continua, Cambridge University Press, 2010.

[19] J. Mosler, Variationally consistent modeling of finite strain plasticity theory with non-linear kinematic hardening, Computer Methods in Applied Mechanics and Engineering. 199 (2010) 2753–2764.

[20] J. Simo, T. Hughes, Computational inelasticity, 7th ed., Springer-Verlag New York. Inc., 1998.

[21] M. Crisfield, Non-linear Finite Element Analysis of Solids and Structures: Volume 1, John Wiley & Sons, Ltd, 1991.

[22] J.C. Simo, R.L. Taylor, Consistent tangent operators for rate-independent elastoplasticity, Computer Methods in Applied Mechanics and Engineering. 48 (1985) 101–118.

[23] T. Belytschko, W. Liu, B. Moran, Nonlinear Finite Elements for Continua and Structures, John Wiley & Sons, Ltd, 2000.

[24] J. Bonet, R.D. Wood, Nonlinear continuum mechanics for finite element analysis, 2nd Editio, Cambridge University Press, 2008.

[25] A. Vinckier, G. Semenza, Measuring elasticity of biological materials by atomic force microscopy, FEBS Letters. 430 (1998) 12–16.

[26] H. Haga, S. Sasaki, K. Kawabata, E. Ito, T. Ushiki, T. Sambongi, Elasticity mapping of living fibroblasts by AFM and immunofluorescence observation of the cytoskeleton, Ultramicroscopy. 82 (2000) 253–258.

[27] L. Sirghi, J. Ponti, F. Broggi, F. Rossi, Probing elasticity and adhesion of live cells by atomic force microscopy indentation, European Biophysics Journal. 37 (2008) 935–945.

[28] S. Hamann, J.F. Kiilgaard, T. Litman, F.J. Alvarez-Leefmans, B.R. Winther, T. Zeuthen, Measurement of Cell Volume Changes by Fluorescence Self-Quenching, Journal of Fluorescence. 12 (2002) 139–145.

[29] E. Zlotek-Zlotkiewicz, S. Monnier, G. Cappello, M. Le Berre, M. Piel, Optical volume and mass measurements show that mammalian cells swell during mitosis, The Journal of Cell Biology. 211 (2015) 765–774.

RESPONSIBILITY NOTICE

The authors are the only responsible for the printed material included in this paper.